analytical chemistry

pubs.acs.org/ac

Article

# Organic Mass Cytometry Discriminating Cycle Stages of Single Cells with Small Molecular Indicators

Shu-Ting Xu, Cheng Yang, and Xiu-Ping Yan*

Cite This: *Anal. Chem.* 2023, 95, 2312−2320

Read Online

ACCESS | Metrics & More | Article Recommendations | Supporting Information

**ABSTRACT:** Cell cycle is a significant factor toward cellular heterogeneity, so cell cycle discrimination is a precise measurement on the top of single-cell analysis. Single-cell analysis based on organic mass spectrometry has received great attention for its unique ability to profile single-cell metabolome, but the influence of cell cycle on cellular metabolome heterogeneity has been overlooked until now due to the lack of a compatible cell cycle discrimination method. Here, we report a robust protocol based on the combination of three small molecular indicators, consisting of two small molecular labels (Hoechst and docetaxel) and one cellular endogenous compound [phosphocholine (34:1)], to discriminate single cells at different cycle stages in real time by organic mass cytometry. More than 6000 HeLa cells were acquired by an improved organic mass cytometry system to build a cell cycle differentiation model. The model successfully discriminated single HeLa cells, SCC7, and Hep G2 cells, at $G_0/G_1$, S, and $G_2/M$ stages with larger than 85% sensitivity and larger than 89% specificity. Along with cell cycle discrimination, obvious heterogeneity of amino acids, nucleotides, energy metabolic intermediates, and phospholipids was observed among single cells at different cycle stages by this protocol, further demonstrating the necessity of cell cycle discrimination for cellular metabolome heterogeneity research and the potential of more endogenous small molecular compounds for cell cycle discrimination.

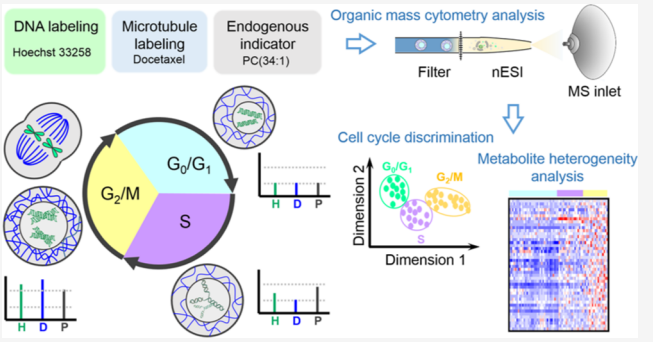




## INTRODUCTION

Mass cytometry based on organic mass spectrometry (MS) is a recently introduced technology for flow cytometric single-cell analysis.[1−3] It is uniquely positioned to measure single-cell metabolome that lies in the most downstream of cellular contents. Single-cell metabolome is considered as the most direct indicator of cell activity.[4] Hundreds of metabolites in single cells detected by organic mass cytometry exhibit obvious differences in various cell subtypes and even more in the same subtype of homologous cells.[2,5,6] Understanding cellular metabolic heterogeneity and its causes are of great meaning for the research of diseases and cell biology.

Among the contributing factors toward cellular heterogeneity, unsynchronized cycle of cells is one of the most important factors that affect the homologous cell phenotypes in the culture and leads to the drug-response, aging, and many other heterogeneous behaviors.[7,8] Homologous cells under the mitotic phase (M phase), $G_0$ phase, $G_1$ phase, DNA synthesis phase (S phase), or $G_2$ phase are significantly different from intracellular active compounds to cellular morphology, and information collected from known specific cell cycle stages is undoubtedly more accurate than average results for disease and cell biology research. Protocols based on cell cycle synchronization before analysis have been employed to analyze cell cycle-related pathways,[9] but the synchronization is time-consuming and might affect the biochemical pathways. Ideally, the natural cell cycle stage needs to be identified in real time for each cell with other cellular information during a high-throughput cytometric analysis.[10]

Mass cytometry based on inductively coupled plasma MS (ICP−MS) is an efficient technology for cell cycle discrimination.[11,12] Protocols have been developed in which 5-iodo-2-deoxyuridine was utilized as an S phase indicator, simultaneously with antibodies against cyclin B1, cyclin A, phosphorylated histone H3 (S28), and phosphorylated retinoblastoma protein (S807 and 811) for $G_0$, $G_1$, $G_2$, and M phases.[13] More than 40 parameter dimensions enable the accurate identification of cell cycle phase with many other intracellular parameters, such as differentiation, activation, and exhaustion markers, to study cancers and other disorders.[14] However, ICP-based mass cytometry is not suited to metabolome measurement, while the protocols based on cell

**Received:** September 21, 2022
**Accepted:** January 9, 2023
**Published:** January 18, 2023

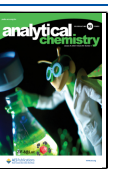

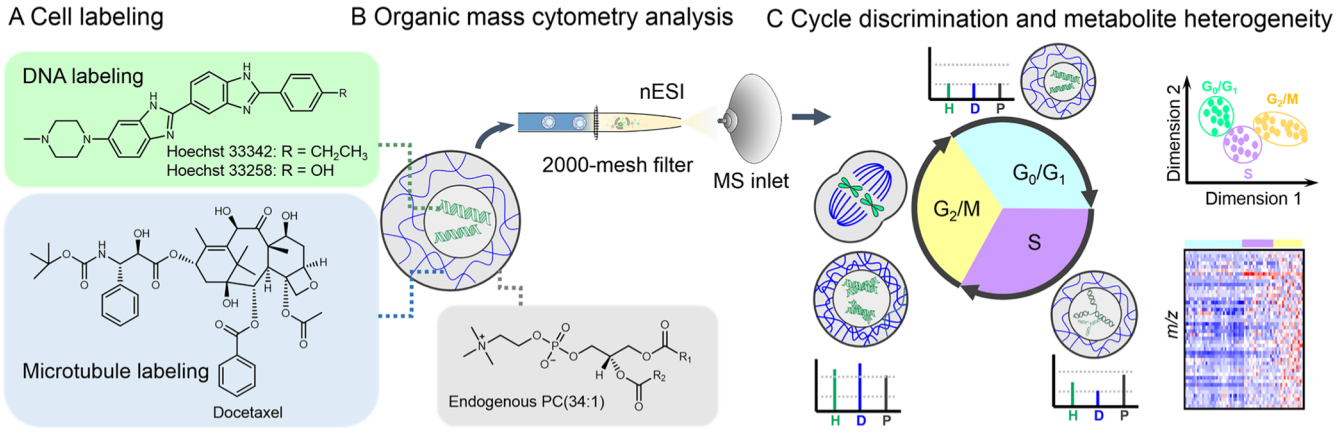


**Figure 1.** Schematic for cell cycle discrimination by organic mass cytometry. (A) Cell labeling with two types of small molecular indicators (Hoechst33258/Hoechst33342 and docetaxel). (B) Single-cell detection by high-throughput organic mass cytometry. (C) Cell cycle discrimination ($G_0/G_1$, S, and $G_2/M$ stages) based on the signals of Hoechst, docetaxel, and endogenous phosphocholine (PC) (34:1) and preliminary metabolite heterogeneity analysis at different cell cycle stages.

fixation and metal-tagged indicators mostly against proteins are incompatible with metabolite labeling and organic mass cytometry system.

Several robust real-time markers to indicate cell cycle stages, represented by propidium iodide, 4′,6-diamidino-2-phenylindole and Hoechst dyes for DNA staining, have also been developed in fluorescent flow cytometry analysis.[15−17] These markers are DNA indicators that can resolve cells with 2n and 4n DNA content before and after S phase. However, their protocols mainly contain cellular permeability operation that causes cellular metabolite loss, and single DNA indicator is always insufficient for accurate cycle stage discrimination. Fluorescent ubiquitination-based cell-cycle indicator (Fucci) and its variants have been developed to fuse with cell cycle-related proteins to resolve four cell cycle stages,[18] but they require protein fusion that takes a long time and are difficult to release during organic MS detection. Furthermore, fluorescence-based cellular metabolite detection is difficult because of limited labels for metabolites and limited channels.[19]

In fact, metabolome difference among cell cycle stages is mostly overlooked during cellular metabolome analysis due to the lack of cell cycle indicators compatible with organic mass cytometry. Because cellular metabolome is highly active, indicators adapted to organic mass cytometry confront with harsher rules than fluorescent flow cytometry and ICP-based mass cytometry: (i) live-cell labeling, (ii) low toxicity and low metabolic perturbation, (iii) highly efficient release/dissociation during ionization, (iv) high response in organic MS, and (v) low signal interference from the biological matrix. Two main directions can be taken into consideration to hunt for cell cycle mass indicators in organic mass cytometry analysis. One direction could be small molecules targeted to cellular contents that significantly change in different cell cycle stages, such as DNA and tubulin. In this regard, although fluorescence techniques are limited in metabolite detection, many existing small fluorescent molecular dyes with good cell membrane penetration for live-cell staining are mass indicator candidates.[20,21] The other direction is endogenous cellular compounds detected in organic mass cytometry as endogenous compounds with cell cycle difference could be natural indicators to identify cell cycle phases.[22]

Here, we explore a combination of three small molecules, including the Hoechst (HOE, small molecular DNA dyes), the docetaxel (DOC, a small molecular drug targeted to polymerized tubulin), and phosphocholine (PC) (34:1) (a cellular endogenous lipid), as mass indicators for real-time discriminating single cells at different cycle stages (Figure 1A). The cell cycle discrimination of single cells is conducted via a high-throughput organic mass cytometry system. This system is developed based on our previous online-lysis organic mass cytometry,[23] and higher throughput to maintain more single-cell acquisition is achieved in one test by the updated system (Figure 1B). Main cell cycle stages, including $G_0/G_1$, S, and $G_2/M$, are discriminated with the combined indicators and the updated organic mass cytometry system (Figure 1C), and cellular metabolome heterogeneity based on cell cycle subtypes are further investigated. This work provides a simple and efficient cell cycle discrimination protocol with small molecular indicators as a prelude to accurate studies of single-cell cycle-related metabolic activity.

## EXPERIMENTAL SECTION

**Apparatus.** An organic mass cytometry system was established for high-throughput single-cell analysis based on our previous work.[23] The setup is shown in Figure S1A. In brief, an external syringe pump with a magnetic stirring device was employed for injecting cells. The cell flow was then mixed with two solvent flows inside the microcrosses. The outlet of microcrosses was connected in turn to a flat-bottom fitting, a stainless-steel adapter, and a nanoelectrospray (nESI) emitter (Figure S1B). A piece of copper 2000-mesh filter with 6.5 $\mu$m bores (G2000HS, Gilder Grids, UK) was placed in the flat-bottom fitting for online cell lysis (Figure S1B inset). The above setup was installed in the holder of Nanospray II Source (AB SCIEX, USA) and placed in front of a commercial QTRAP@4500 mass spectrometer (AB SCIEX, USA).

**Cell Labeling and Organic Mass Cytometry Analysis.** The harvested cells, including synchronized cells and normal cultured cells in 1 mL Dulbecco's phosphate-buffered saline (DPBS) with a concentration of $10^6$ cells/mL, were labeled by HOE33258 (or HOE33342) and DOC. The optimal final concentrations of HOE33342, HOE33258, and DOC were 15 $\mu$g/mL, 25 $\mu$g/mL, and 600 ng/mL, respectively. The cell suspension with DOC was incubated in dark at 37 °C for 5 min with gentle shaking followed by the addition of HOE33258 (or HOE33342) and incubated for 5 min more.


https://doi.org/10.1021/acs.analchem.2c04165
Anal. Chem. 2023, 95, 2312−2320

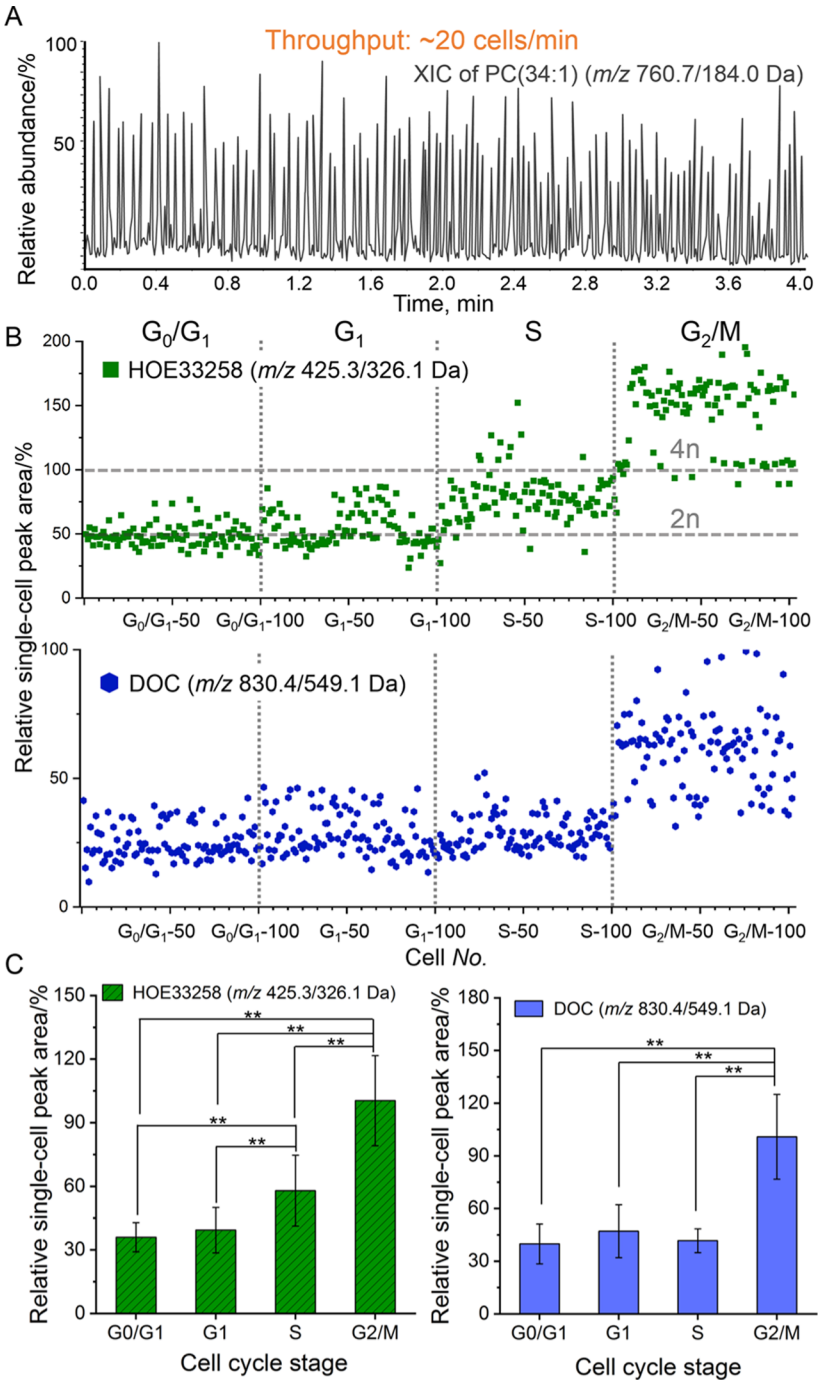


**Figure 2.** (A) Extracted ion chromatogram (XIC) of PC(34:1) ($m/z$ 760.7/184.0 Da) for the detection of ~2 × $10^4$/mL cells with the naked 2000-mesh filter (cell suspension, 1 $\mu$L/min; methanol, 4 $\mu$L/min). (B) Single-cell signal variability of HOE33258 ($m/z$ 425.3/326.1 Da) and DOC ($m/z$ 830.4/204.1 Da) in HeLa cells at four synchronized cycle stages ($G_0/G_1$, $G_1$, S, and $G_2$/M). 2$n$: the theoretical 2$n$ DNA contents; 4$n$ (100%): the theoretical highest 4$n$ DNA contents. (C) Average HOE33258 and DOC signal abundance in HeLa cells at four synchronized cycle stages. Error bars: One standard deviation for about 1500 single-cell peak areas. Four groups of average signal abundance in HeLa cells at four synchronized cycle stages were compared with each other by TTEST (**: $P$ value < 0.01).

Cells were then washed with DPBS three times and finally resuspended in ammonium formate aqueous solution (140 mmol/L, pH 7.3).

For organic mass cytometry analysis, multiple reaction monitoring (MRM), full scan (Q1), and product ion (MS2) modes were employed under optimal parameters (Table S1). For the MRM mode, cell suspensions (about 2 × $10^4$/mL) were injected with a flow rate of 1 $\mu$L/min, and methanol with internal standard (IS) (36 nmol/L rhodamine B) was injected simultaneously as online extraction solvent with a flow rate of 4 $\mu$L/min. Twenty precursor ion/product ion pairs of labeling reagents, cellular lipids, and IS were monitored in MRM (Table S2). For Q1 and MS2 modes, cell suspensions were further diluted by ammonium formate aqueous solution to 5000 cells/mL with the same flow rate and extraction solvent as the MRM mode.

**Single-Cell Data Analysis.** Data analysis was conducted with Analyst software (version 1.6.3). For the MRM mode, the


https://doi.org/10.1021/acs.analchem.2c04165
Anal. Chem. 2023, 95, 2312−2320

signals of HOE33258 ($m/z$ 425.3/326.1 Da), HOE33342 ($m/z$ 453.4/396.1 Da), DOC ($m/z$ 830.4/549.1 Da), and PC(34:1) ($m/z$ 760.7/184.0 Da) were calibrated with IS ($m/z$ 443.2/399.2 Da) to obtain calibrated single-cell peak areas for semi-quantification. The single-cell peaks were filtrated by PC(34:1) signals as PC(34:1) signals below 30% or larger than three times of the mean value were excluded to avoid cell debris or clusters. For synchronized cells, pulse-like signals out of 95% confidence interval around the mean value were excluded to avoid unsynchronized cells.

For metabolite-related analysis in Q1 and MS2 modes, mass spectra were first recorded from the single-cell peaks in the Q1 mode. Potential metabolite signals in the Q1 mode were then analyzed in MS2 modes. The precursor and product ions were referred to human metabolome database (HMDB) for metabolite assignment. The single-cell peak areas of assigned metabolites, HOE33258 and DOC in Q1 mode, were calibrated with IS ($m/z$ 443.2 ± 0.3 Da) for semi-quantification. Abundance of precursor ions for HOE33258, DOC, and PC(34:1) in the Q1 mode were corrected with the abundance of their precursor ion/product ion pairs in the MRM mode for cell cycle discrimination.

The cell clusters for different cell cycle stages were visualized by the principal component analysis (PCA) (SIMCA 14.1). The cell cycle discrimination ability of different indicator data sets was evaluated by the hierarchical clustering analysis (Ward's method, square Euclidean distance; SPSS 23).

## RESULTS AND DISCUSSION

**High-Throughput Single-Cell Screening by Organic Mass Cytometry.** Flow cytometric mode is a breakthrough progress to organic MS techniques for single-cell analysis with dozens of cells per minutes to acquire statistically significant data.[1,2] Our previous work has established an online-lysis mass cytometry system with a nanostructure-decorated filter to further enhance the signal response of intracellular and intranuclear compounds by deep cell lysis.[23] However, the nanostructures on the filter for cell rupture have inevitable contamination that requires washing after a period of detection (about 20 min), and the deep cell lysis causes the long signal duration for each cell (about 7 s). Therefore, only about 100 cells can be acquired in one sample, which is still looking forward to continuous high throughput.

In this work, we explored the naked small-bore filter to improve the throughput of online-lysis organic mass cytometry system for single continuous test. The naked 2000-mesh filter with 6.5 μm bores has well acceptable cell lysis degree of an average eightfold signal enhancement of intracellular and intranuclear signals compared with no filter.[23] Here, the naked filter further presented its advantage for long-period continuous detection compared with sharp-nanostructure-decorated filter. We continuously performed organic mass cytometry for the mixture of HOE33258 labeled cells and unlabeled cells for about 60 min with naked 2000-mesh filter. The filter remained its complete mesh structure with few sample contaminations after analysis (Figure S2). The signal of HOE33258 had no signal residue to the unlabeled cells using PC(34:1) to display single-cell peaks during a 60 min detection period (Figure S3), demonstrating the low sample contamination and long useful life as well as acceptable single-cell sensitivity of naked 2000-mesh filter.

We also employed high flow rate to further improve the cell throughput. The total flow rate was investigated from 1 to 7 μL/min with a constant optimal solvent proportion of 80% (Figure S4). The moderate flow rate of 3 μL/min gave the highest single-cell peak areas based on the accumulated signal of PC(34:1) and HOE33258 with about 6 s single-cell duration (Figure S5). Although the cell signals were slightly lower at the flow rate of 4 or 5 μL/min, 5 μL/min led to the increased throughput to more than 10 cells/min. In addition, the short single-cell duration of 1.8 s at a total flow rate of 5 μL/min could afford a higher throughput to about 20 cells/min with the injecting cell concentration of $2 \times 10^4$ cells/mL. Higher flow rate of 7 μL/min caused poor signal-to-noise ratio (S/N) and single-cell distinction because of the decreased single cell sensitivity (Figure S5). Comprehensively considering the signal intensity and throughput, a total flow rate of 5 μL/min was finally adopted for further analysis, achieving a cell throughput of about 20 cells/min (Figure 2A) for the MRM mode.

The cellular state during detection was investigated to ensure the valid cytometric acquisition time. The cell activity in the organic-MS-compatible ammonium formate aqueous solution (140 mmol/L, pH 7.3) was tested in a period from 10 to 60 min. The cell viability decreased to less than 85% after the cells were suspended in ammonium formate solution for more than 30 min (Figure S6A). The leakage of cell content was another problem after long-period detection. The background signals of HOE33258 and PC(34:1) increased rapidly after 30 min continuous detection (Figure S6B), and the S/N ratios of single-cell peaks obviously decreased after 30 min (Figure S7). As a result, the first 30 min acquired cell information is more reliable although the long useful life filter and high flow rate ensured a long-period cell detection up to 60 min. Thus, a total 30 min detection time was employed, and about 600 single-cell data could be acquired under the optimal condition, which was 10 times more than our previous work.[23]

The repeatability of the organic mass cytometry system was demonstrated by comparing parallel samples from repeated detections. There was no distinction among three parallel cell samples detected with the same filter (Figure S8A). The commercial mesh filters were replaceable and ensured good batch repeatability. Three parallel samples also had no distinction using three filters taken at random (Figure S8B). Good repeatability further improved the applicability of the organic mass cytometry system for cell biology application.

**Cell Cycle Indicating by Small Molecular Labels.** Small molecular indicators have better compatibility with organic MS than metal-based indicators.[24] However, small molecular indicators are difficult to find an effective intracellular target. On-demand dissociation of indicators is another problem during the ionization of organic MS analysis. DNA and tubulin, which have the most direct correlation with cell cycle,[25] were focused as the targets of indicators, and some commercial DNA dyes and tubulin-related drugs were extended as mass indicators for cell cycle indicating.

HOE reagents are a series of popular DNA fluorescent dyes that can embed in the minor grooves of double-strand DNA.[26] HOE can penetrate living cell membranes, so they are generally applied for living cell labeling and have low toxicity for cells at the μg/mL level during a few minutes. The noncovalent bonding between HOE and DNA is convenient for dissociation during MS detection, and the HOE structures have permanent positive charges, making these molecules easily generate high MS response.


https://doi.org/10.1021/acs.analchem.2c04165
Anal. Chem. 2023, 95, 2312−2320

Representative HOE, HOE33258, was first tested for living cell labeling and organic mass cytometry detection. As a prerequisite for MS detection, we demonstrated that the calibrated signal intensities of HOE33258 were linear with their concentrations in cell lysis matrix with low matrix interference (Figure S9A and Table S3). Then, the labeling conditions adapted to MS analysis were investigated. Concentration from 1 to 30 $\mu$g/mL was tested for cell labeling, and the incubation time was optimized from 5 to 20 min. HOE33258 reached the highest S/N with the incubation concentration of 25 $\mu$g/mL (Figure S10A), and 5 min incubation time was enough to label cells to achieve the highest S/N (Figure S10B).

The HOE33258 signals among different cell cycle stages were focused to investigate their ability for cycle stage discrimination. For clear comparison, HeLa cells were synchronized to specific cycle stages ($G_0/G_1$, late $G_1$, S, and $G_2$/M). The synchronized cells were demonstrated by microscope observation and fluorescent flow cytometry. Most $G_2$/M cells showed obvious morphological changes (Figure S11) conforming to the mitosis characteristic.[27] The fluorescent flow cytometry further validated the nearly multiple increases of HOE33258 signals from $G_0/G_1$ and S to $G_2$/M cells corresponding to theoretically $2n$, $2n-4n$, and $4n$ DNA contents in these stages, respectively (Figure S12).

For organic mass cytometry analysis, the HOE33258 signals also presented gradual increase for single cells from $G_0/G_1$ and S to $G_2$/M stages (Figure 2B,C), and most $G_0/G_1$ cells and S cells had the $2n$ and $2n-4n$ quantitative relationship. However, only a part of $G_2$/M cells displayed nearly $4n$ abundance, while most $G_2$/M phase cells were more than the double of $G_0/G_1$ signals (Figure 2B). It is hard to understand the results in term of original DNA content. We tried to find explanation from other cell cycle characteristics. The nuclear membrane was found ruptured when cells entered the M phase (Figure S13A), so the disappeared nuclear membrane could lead to a higher release efficiency of HOE33258 during online cell lysis and extraction. With the help of efficient release, the intensities of HOE33258 for M phases could have higher response larger than $4n$, and the normal $4n$ cells were probable to be $G_2$ cells that still had intact nuclear membranes. These signal differences were unique based on the online-lysis organic mass cytometry system, and had potential to resolve $G_2$ and M cells with the same DNA content. Cells with more than fivefold HOE33258 abundance than $G_0/G_1$ cells were mainly apoptotic cells without membrane barrier,[28] which were excluded for further analysis to guarantee the accuracy of single-cell data. Another HOE dye, HOE33342 displayed similar results for cell cycle discrimination as HOE33258 (Figure S14) with optimal conditions (Figure S10), indicating the potential of all HOE dye series for organic mass cytometric use.

The HOE differentiation in different cycle stages was verified by high performance liquid chromatography (HPLC)-MS/MS based on a large amount of cells (Tables S4 and S5 and Figure S15). In addition, two cell extraction approaches, including fast vortex extraction and deep ultrasonication extraction were compared to simulate the online single-cell extraction and extraction after cell lysis, respectively (Figure S15). Higher HOE response was obtained after deep ultrasonication extraction compared to fast vortex extraction for $G_0/G_1$ and S stage cells, while the increasing for $G_2$/M stage cells was not in high degree. The HPLC-MS/MS results illustrated the easy release of HOE in $G_2$/M stage cells due to the lack of nuclear membrane in M cells.

Docetaxel, a commonly used chemotherapy drug, is targeted to polymerized tubulin with non-covalent bonding.[29] It has been used as the microtubule markers during the fluorescent imaging of microtubule when docetaxel is coupled with fluorophores.[30] Here, we tried to expend it as a mass marker to indicate the cellular microtubule content. The docetaxel signal can be directly used as the indicator because there is no interference from endogenous signals against the semi-quantification of docetaxel in cell lysis extract (Figure S9B).

The incubation concentration and time of DOC as a mass indicator for cell labeling were systematically optimized. Relative low concentration and short time were preferred to make the labeling process highly efficient and low cellular perturbation. The concentration was optimized from 100 to 800 ng/mL with an incubation time from 5 to 30 min. The S/N of DOC achieved the highest after the incubation of 600 ng/mL DOC for 10 min (Figure S16).

With the optimal condition, the $G_0/G_1$/S phase cells presented similar response of DOC, while $G_2$/M cells achieved the highest intensities (more than twofold larger than $G_0/G_1$/S phase cells) (Figure 2B,C). High DOC response in the $G_2$ phase could be attributed to the large amount of tubulin that synthesized and polymerized in this phase to form spindle for mitosis.[31] The signal trends among four cell cycle stages were verified in a large number of cells by HPLC-MS/MS (Figure S17) and fluorescent flow cytometry with commercial dye based on docetaxel (Figure S18). The results further proved the highest intensities of DOC-related reagents in $G_2$/M cells.

The HOE and DOC indicators were then combined for cell labeling, and the cytotoxicity of the combined indicators was evaluated by cell viability. The simultaneous labeling by the two indicators was low cytotoxicity because the labeled cells maintained more than 90% cell viability after 10 min labeling (Figure S19A). The labeled cells could further maintain more than 85% viability during the 30 min suspending in ammonium formate solution after labeling, covering the whole MS detection period (Figure S19B). In addition, HOE and DOC labeled cells almost had no distinction in cellular content compared with unlabeled cells, demonstrating the little perturbation of labels for cellular metabolism (Figure S20B). The single-cell signals of HOE and DOC also presented good stability during the 30 min MS detection (Figure S20A). Therefore, the HOE and DOC were qualified to be cell cycle indicators for organic mass cytometry and provided high chance to distinguish different cell cycle stages.

However, single HOE, single DOC, and combined HOE and DOC all resulted in poor sensitivity (<75.5%), especially between $G_0/G_1$ and S stages (Table S6 and Figure S21). Combination of more indicators was then considered to achieve more accurate discrimination.

**Endogenous Indicators for Cell Cycle Discrimination.** Lipids, the cellular endogenous compounds, were investigated as assistant cell cycle indicators. Lipids are the most detectable compounds by organic mass cytometry in single cells and closely associated with cellular morphology, viability, and activity.[3,32] We investigated the lipid variation among different cell cycles based on PC(34:1) that was the representative lipid with the highest response in single cells. An obvious increase of PC(34:1) intensity was observed from the $G_1$ phase to S phase, and the cells under $G_2$/M phase also presented a small increase in PC(34:1) (Figure 3A,B). The trends of PC(34:1) in these


https://doi.org/10.1021/acs.analchem.2c04165
Anal. Chem. 2023, 95, 2312−2320

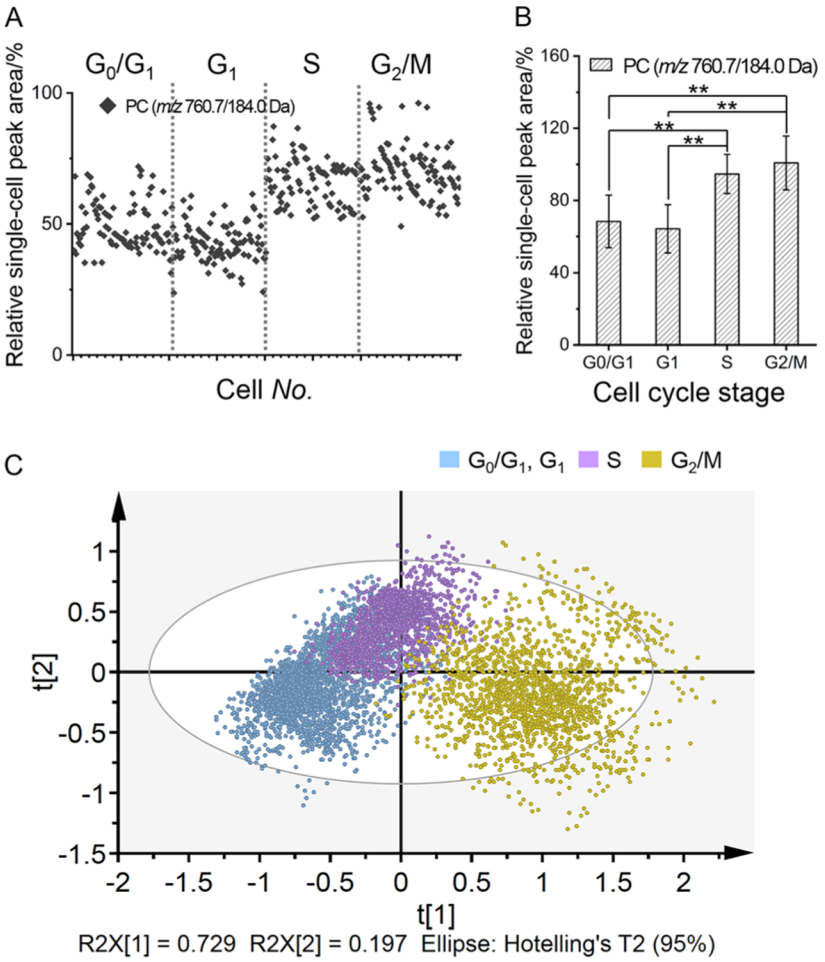


**Figure 3.** (A) Single-cell signal variability of PC(34:1) ($m/z$ 760.7/184.0 Da) for HeLa cells at four synchronized cycle stages ($G_0/G_1$, $G_1$, S, and $G_2$/M). (B) Average PC(34:1) signal abundance in HeLa cells at four synchronized cycle stages. Error bars: One standard deviation for about 1500 single-cell peak areas. Four groups of average signal abundance in HeLa cells at four synchronized cycle stages were compared with each other by TTEST (**: $P < 0.01$). (C) PCA of HeLa cells under synchronized cycle phases [$G_0/G_1(G_1)$, S, and $G_2$/M] based on HOE33258, DOC, and PC(34:1) [R2X[1] = 0.729, R2X[2] = 0.197, summarized percent of variation explanation: 92.6%, noise removed: 7.4%].

cell cycle semi-quantified by HPLC-MS with cell populations were consistent with the increase trends from $G_0/G_1$ to $G_2$/M phase (Figure S22).

Factors for the increase of PC(34:1) in different cycle stages were discussed. We first considered the reason based on cell size. For many types of mammalian cells, such as CHO cells and K562 human erythroleukemia cells, the $G_0/G_1$ and early S cells are smaller than the middle/late S and $G_2$/M cells.[33] We measured the HeLa cell size of different cycle stages, and found that S and $G_2$/M cells gave larger diameter than $G_0/G_1$ cells by 12.3 and 21.1% (Figure S13). The size of nucleus also became larger along with the DNA synthesis process under the S phase, and the nuclear membrane ruptured in M phase. The larger size of cells and nuclear of S and $G_2$/M cells suggested the increase of PC(34:1) content at these cycle stages. There could be another reason for the high PC(34:1) signal based on the size-dependent lysis degree and signal response via organic mass cytometry. The larger size of cells and nucleus could result in the more efficient lysis to achieve a higher response of cellular compounds. Lipids in larger cells and nucleus had increased amount and were more efficiently lysed, both contributing to the increase of PC(34:1) signals from $G_0/G_1$ to $G_2$/M. Therefore, the signal of PC(34:1) could be employed as an endogenous indicator for cell cycle discrimination, and made great contribution to discriminating the $G_0/G_1$ and S cells.

**Combined Indicators for Cell Cycle Discrimination.** The differentiations of three indicators [HOE, docetaxel and PC (34:1)] among different cell cycle phases were finally combined to distinguish and identify the main cycle stages of HeLa cells. The information of more than 6000 cells belonging to four synchronized cell cycle stages were acquired to establish the cell cycle discrimination model. The $G_0/G_1$ phases and late $G_1$ phase cells had no distinction in PCA (Figure S23) because the cells in these phase were similar in most cell behaviors, such as the DNA and tubulin contents and cell cellular morphology. Thus, these two groups were considered as one stage.

Finally, three cell cycle stages, $G_0/G_1(G_1)$, S, and $G_2$/M, were successfully distinguished by the three combined indicators (Figure 3C). The average sensitivity and specificity were significantly improved to about 85% and larger than 90%, respectively (Table S6). Both HOE33342 and HOE33258 were efficient for the cell cycle differentiation, and the HOE33258 presented a little bit higher sensitivity and specificity than HOE33342 (Table S6). Therefore, the combination of HOE33258, DOC, and PC(34:1) was preferred to as the final cell cycle indicators adapted to organic


https://doi.org/10.1021/acs.analchem.2c04165
Anal. Chem. 2023, 95, 2312−2320

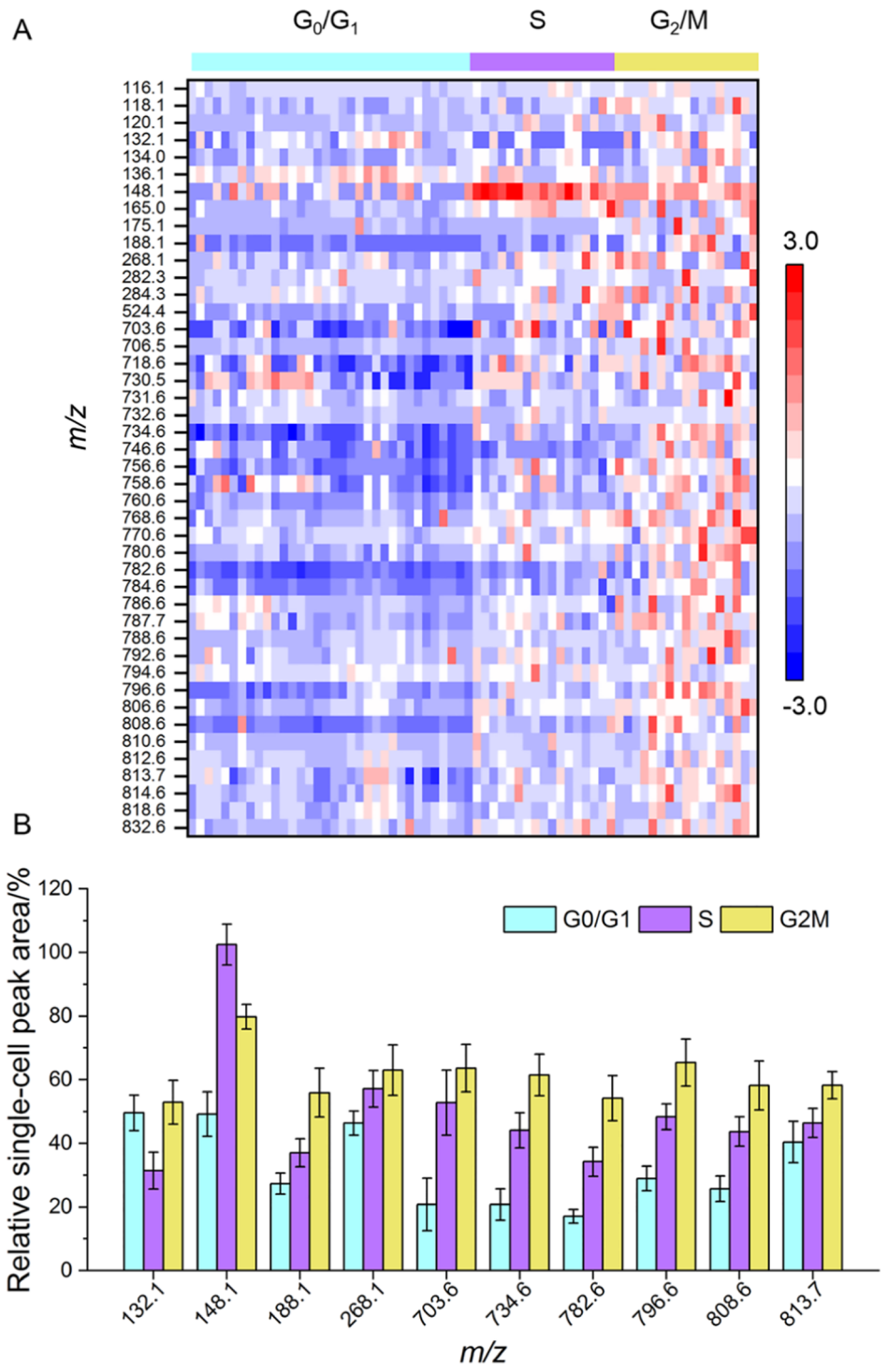


**Figure 4.** (A) Heatmap of the single HeLa cell endogenous compounds (44 signals assigned to cellular metabolites within $m/z$ 100−1000 Da) at three cell cycle stages ($G_0/G_1$, S, and $G_2/M$). (B) Average abundance of 10 assigned signals in single HeLa cells at three cell cycle stages ($G_0/G_1$, S, and $G_2/M$). Error bars: One standard deviation for about 150 single-cell peak areas.

mass cytometry analysis. This discrimination degree was sufficient for many cell biology research based on specific cell cycles, such as the drug-induced cell proliferation perturbation (S and $G_2/M$ stages), and cell apoptosis/autophagy ($G_0$ and $G_1$ stages).[34−36] Moreover, the $G_2/M$ and S stage cells displayed multiple potential subtype clusters in PCA analysis after hierarchical clustering (Figures S24, S25, and S25). The subtypes in $G_2/M$ stages were high probable to be $G_2$ and M according their differences in HOE abundance, and subtype in S stage might be some intra S stages,[37] indicating a high potential of organic mass cytometry for finer cycle discrimination.

The feasibility and versatility of the cell cycle discrimination model based on HeLa cells were investigated by expanding this model to other cell lines. Two cell lines, including SCC7 cells belonging to mouse squamous cell carcinoma cell line and Hep G2 cells belonging to human liver cancer cell line, were analyzed following the same protocol as HeLa cells. The results


https://doi.org/10.1021/acs.analchem.2c04165
Anal. Chem. 2023, 95, 2312−2320

demonstrated that SCC7 cells and Hep G2 cells presented similar signal trends of indicators as HeLa cells for different cell cycle stages (Figure S26). Although the signal abundance values of three indicators in three cell types were different (Figure S27), these values could be unified by using correction factors. For SCC7 cells, correction factors as 0.914, 0.769, and 0.871 were used for HOE33258, DOC, and PC(34:1), respectively. For Hep G2 cells, correction factors as 0.996, 0.702, and 0.766 were used for HOE33258, DOC, and PC, respectively. After using correction factors, the HeLa cell cycle discrimination model was successfully expanded to SCC7 cells and Hep G2 cells (Figure S28), achieving large than 87% sensitivity and larger than 89% specificity (Table S7). These results demonstrated that this protocol had high feasibility and versatility for cell cycle discrimination of different types of cells.

The regular unsynchronized HeLa cells were tested to further verify the identification of unknown cell cycle stages by this protocol. Nine groups of normal cultured HeLa cells were harvested at three different growth periods (8, 16, and 24 h). As a result, each unknown HeLa cell among huge cell populations was efficiently assigned to different cell cycle stages in real time (Figure S29). The cell proportions presented high amount of S, $G_2$, and M stage cells after 16 h growth, and the largest amount of $G_0/G_1$ cells at 8 and 24 h (Table S8). Compared to the 24 h doubling time of HeLa cells (about 12 h in $G_1$ stage, 8 h in S stage, 2 h in $G_2$ stage, and 1 h in M stage)[38] and fluorescent flow cytometry results (Figure S30 and Table S8), the protocol based on three combined indicators and organic mass cytometry presented high reliability for real-time cell cycle identification, and it was the basis for metabolome heterogeneity analysis in special cycle stages.

**Metabolite Heterogeneity Based on Cell Cycle Subtypes.** The nearly unfettered detectable channels of organic mass cytometry have the ability for simultaneous acquisition of abundant cellular endogenous small molecules with cell cycle indicators (Table S9). To this point, a preliminary untargeted scan ($m/z$ 100−1000 Da) of intracellular small molecules in single cells was performed with indicators to study metabolite heterogeneity in single cells with specific cycle stages. About 44 signals were preliminarily assigned as cellular metabolites, including amino acids, nucleotides, energy metabolic intermediates, and phospholipids, based on their fragment ions in the MS2 mode in single HeLa cells (Table S10).

Many of these assigned signals in single HeLa cells presented obvious heterogeneity at different cell cycle stages ($G_0/G_1$, S, and $G_2$/M) (Figure 4A). Among these heterogeneous signals, $m/z$ 148.1 (assigned to glutamic acid), $m/z$ 188.1 (assigned to 3-indoleacrylic acid), $m/z$ 268.1 (assigned to adenosine), and many phospholipids displayed obvious increase in S and $G_2$/M stages compared with $G_0/G_1$ stages (Figure 4B), might indicating a more active state and morphologic change of cells in S and $G_2$/M stages. All these differences in metabolites among cell cycle stages demonstrate the necessity of cell cycle identification with metabolome analysis. Our protocol provides the opportunity to investigate the metabolic pathways based on a more meticulous cell sub-groups and build relationships between metabolic pathways with cell cycle stages.

On the other hand, the large natural heterogeneous intracellular compounds are all endogenous candidates to be cell cycle mass indicators. Based on these assigned metabolite signals, the main three cell cycle stages were also successfully discriminated (Figure S31). After further identification and verification of intracellular compounds, more endogenous heterogeneous indicators could be employed to achieve more accurate and fine cell cycle discrimination.

## CONCLUSIONS

In summary, we have developed a simple and efficient protocol for cell cycle discrimination and identification using a combination of three small molecular indicators, including exogenous labels (HOE and DOC) and endogenous PC(34:1). These small molecular indicators not only have high compatibility with organic mass cytometry analysis but also give the advantages of low toxicity and low metabolic perturbation for living-cell labeling, high sensitivity for single-cell detection, and obvious signal differentiation for cell cycle discrimination. More than 6000 HeLa cells have been acquired via the developed high-throughput organic mass cytometry system to establish a large single-cell database for cycle discrimination. Main cell cycles, including the $G_0/G_1$, S, and $G_2$/M phases, have been discriminated with high sensitivity and specificity, and the discrimination model based on HeLa cells has been expanded to other cell lines. Preliminary metabolome heterogeneity has been observed among cells at specific stages, demonstrating the necessity of cell cycle discrimination during single-cell analysis. New perspectives have been proposed to discover more endogenous indicators and employ high resolution and high-throughput MS for the analysis of single-cell metabolome and metabolic pathways within the more precise cell cycle subtypes.

## ASSOCIATED CONTENT

### Supporting Information

The Supporting Information is available free of charge at https://pubs.acs.org/doi/10.1021/acs.analchem.2c04165.

Additional experimental details for chemicals; cell culture and synchronization; cell viability test; HPLC-MS/MS analysis; fluorescent imaging and fluorescent flow cytometry detection; MS and HPLC parameters; optimization results of organic mass cytometry system and HOE and DOC labeling; characterization of cell state during detection; fluorescent images and fluorescent flow cytometric results; HPLC-MS/MS results of HOE, DOC, and PC(34:1) amounts in HeLa cell populations; results of average HOE, DOC, and PC(34:1) amounts in single SCC7 and Hep G2 cells; and PCA and hierarchical clustering results of cell cycle subtypes (PDF)

## AUTHOR INFORMATION


### Corresponding Author

**Xiu-Ping Yan** − *State Key Laboratory of Food Science and Technology, Jiangnan University, Wuxi 214122, China; International Joint Laboratory on Food Safety, Institute of Analytical Food Safety, School of Food Science and Technology, and Key Laboratory of Synthetic and Biological Colloids, Ministry of Education, Jiangnan University, Wuxi 214122, China;* orcid.org/0000-0001-9953-7681; Email: xpyan@jiangnan.edu.cn

### Authors

**Shu-Ting Xu** − *State Key Laboratory of Food Science and Technology, Jiangnan University, Wuxi 214122, China;*




https://doi.org/10.1021/acs.analchem.2c04165
Anal. Chem. 2023, 95, 2312−2320

*International Joint Laboratory on Food Safety and Institute of Analytical Food Safety, School of Food Science and Technology, Jiangnan University, Wuxi 214122, China*

**Cheng Yang** − *State Key Laboratory of Food Science and Technology, Jiangnan University, Wuxi 214122, China; International Joint Laboratory on Food Safety and Institute of Analytical Food Safety, School of Food Science and Technology, Jiangnan University, Wuxi 214122, China*

Complete contact information is available at: https://pubs.acs.org/10.1021/acs.analchem.2c04165

### Notes

The authors declare no competing financial interest.

## ■ ACKNOWLEDGMENTS

This work was financially supported by the National Natural Science Foundation of China (nos. 22104044 and 21775056), the Natural Science Foundation of Jiangsu Province, China (no. BK20210448), the National First-class Discipline Program of Food Science and Technology (no. JUFSTR20180301), and Collaborative Innovation Center of Food Safety and Quality Control in Jiangsu Province.

## ■ REFERENCES

(1) Yao, H.; Zhao, H. S.; Zhao, X.; Pan, X. Y.; Feng, J. X.; Xu, F. J.; Zhang, S. C.; Zhang, X. R. *Anal. Chem.* **2019**, *91*, 9777−9783.
(2) Xu, S. T.; Liu, M. X.; Bai, Y.; Liu, H. W. *Angew. Chem., Int. Ed.* **2021**, *60*, 1806−1812.
(3) Zhang, W. F.; Li, N.; Lin, L.; Huang, Q. S.; Uchiyama, K.; Lin, J. M. *Small* **2020**, *16*, 1903402.
(4) Zenobi, R. *Science* **2013**, *342*, 1243259.
(5) Shen, Z. Z.; Zhao, H. S.; Yao, H.; Pan, X. Y.; Yang, J. L.; Zhang, S. C.; Han, G. J.; Zhang, X. R. *Chem. Sci.* **2022**, *13*, 1641−1647.
(6) Yao, H.; Zhao, H. S.; Pan, X. Y.; Zhao, X.; Feng, J. X.; Yang, C. D.; Zhang, S. C.; Zhang, X. R. *Anal. Chem.* **2021**, *93*, 10282−10291.
(7) Yang, S.; Cho, Y.; Jang, J. *BMB Rep.* **2021**, *54*, 505−515.
(8) Kar, S. *Cell Syst.* **2016**, *2*, 8−10.
(9) Bordhan, P.; Razavi Bazaz, S.; Jin, D.; Ebrahimi Warkiani, M. *Lab Chip* **2022**, *22*, 445−462.
(10) Dovichi, N. J.; Hu, S. *Curr. Opin. Chem. Biol.* **2003**, *7*, 603−608.
(11) Spitzer, M. H.; Nolan, G. P. *Cell* **2016**, *165*, 780−791.
(12) Darzynkiewicz, Z. *Cytometry, Part A* **2012**, *81*, 546−548.
(13) Behbehani, G. K.; Bendall, S. C.; Clutter, M. R.; Fantl, W. J.; Nolan, G. P. *Cytometry, Part A* **2012**, *81*, 552−566.
(14) Corneau, A.; Cosma, A.; Even, S.; Katlama, C.; Le Grand, R.; Frachet, V.; Blanc, C.; Autran, B. *Cytometry, Part B* **2017**, *92*, 21−32.
(15) Nair, A.; Manohar, S. M. *Bioanalysis* **2021**, *13*, 1627−1644.
(16) Roukos, V.; Pegoraro, G.; Voss, T. C.; Misteli, T. *Nat. Protoc.* **2015**, *10*, 334−348.
(17) Ghosh, K. K.; Jeong, Y. M.; Kang, N. Y.; Lee, J.; Diana, W. S. Y.; Kim, J. Y.; Yoo, J.; Kim, D.; Kim, Y. K.; Chang, Y. T. *Chem. Commun.* **2015**, *51*, 9336−9338.
(18) Bajar, B. T.; Lam, A. J.; Badiee, R. K.; Oh, Y. H.; Chu, J.; Zhou, X. X.; Kim, N.; Kim, B. B.; Chung, M. Y.; Yablonovitch, A. L.; Cruz, B. F.; Kulalert, K.; Tao, J. J.; Meyer, T.; Su, X. D.; Lin, M. Z. *Nat. Methods* **2016**, *13*, 993−996.
(19) Benoist, C.; Hacohen, N. *Science* **2011**, *332*, 677−678.
(20) Kurzawa, L.; Morris, M. C. *Chembiochem* **2010**, *11*, 1037−1047.
(21) Pasquier, E.; Kavallaris, M. *IUBMB Life* **2008**, *60*, 165−170.
(22) Comi, T. J.; Do, T. D.; Rubakhin, S. S.; Sweedler, J. V. *J. Am. Chem. Soc.* **2017**, *139*, 3920−3929.
(23) Xu, S. T.; Yang, C.; Yan, X. P. *Anal. Chem.* **2021**, *93*, 15677−15686.
(24) Liu, R.; Zhang, S. X.; Wei, C.; Xing, Z.; Zhang, S. C.; Zhang, X. R. *Acc. Chem. Res.* **2016**, *49*, 775−783.
(25) Imoto, Y.; Yoshida, Y.; Yagisawa, F.; Kuroiwa, H.; Kuroiwa, T. *J. Electron. Microsc.* **2011**, *60*, S117−S136.
(26) Bucevicius, J.; Lukinavicius, G.; Gerasimaite, R. *Chemosensors* **2018**, *6*, 18.
(27) Zheng, Y. X. *Nat. Rev. Mol. Cell Biol.* **2010**, *11*, 529−535.
(28) Achilles, J.; Harms, H.; Müller, S. *Cytometry, Part A* **2006**, *69*, 173−177.
(29) Imran, M.; Saleem, S.; Chaudhuri, A.; Ali, J.; Baboota, S. *J. Drug Deliv. Sci. Technol.* **2020**, *60*, 101959.
(30) Lukinavičius, G.; Mitronova, G. Y.; Schnorrenberg, S.; Butkevich, A. N.; Barthel, H.; Belov, V. N.; Hell, S. W. *Chem. Sci.* **2018**, *9*, 3324−3334.
(31) Dumontet, C.; Durán, G. E.; Steger, K. A.; Murphy, G. L.; Sussman, H. H.; Sikic, B. I. *Cell Motil Cytoskeleton* **1996**, *35*, 49−58.
(32) Huang, Q. S.; Mao, S. F.; Khan, M.; Li, W. W.; Zhang, Q.; Lin, J. M. *Chem. Sci.* **2020**, *11*, 253−256.
(33) Banfalvi, G. *Nat. Protoc.* **2008**, *3*, 663−673.
(34) Lanzilli, G.; Fuggetta, M. P.; Tricarico, M.; Cottarelli, A.; Serafino, A.; Falchetti, R.; Ravagnan, G.; Turriziani, M.; Adamo, R.; Franzese, O.; Bonmassar, E. *Int. J. Oncol.* **2006**, *28*, 641−648.
(35) Malumbres, M.; Barbacid, M. *Nat. Rev. Cancer* **2009**, *9*, 153−166.
(36) Wang, Y.; Xu, W. B.; Yan, Z. X.; Zhao, W. L.; Mi, J. Q.; Li, J. M.; Yan, H. *J. Exp. Clin. Cancer Res.* **2018**, *37*, 63.
(37) Lambert, W. C.; Kuo, H. R.; Ramos, N. I. *J. Invest. Dermatol.* **1996**, *106*, 347.
(38) Das, A. B.; Loying, P.; Bose, B. *Cancer Lett.* **2012**, *318*, 189−198.